

Photodegradation kinetics and halogens release of the emerging concern pollutants dexamethasone and S-metolachlor on TiO₂/rGO composites

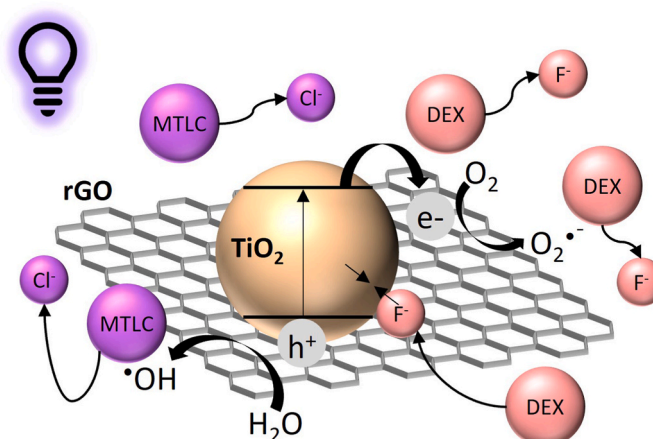
Carmen Barquín, María J. Rivero, Inmaculada Ortiz*

Departamento de Ingenierías Química y Biomolecular, Universidad de Cantabria, Avda. Los Castros, s/n, 39005, Santander, Spain

HIGHLIGHTS

- Photocatalytic degradation of the halogenated MTLC and DEX with TiO₂/rGO is studied.
- The presence of rGO highly improves the degradation rates of MTLC and DEX.
- The released halogen ions matched the concentration of degraded pollutants.
- It is postulated that with TiO₂/rGO there are no halogenated intermediates.

GRAPHICAL ABSTRACT



ARTICLE INFO

Handling editor: S Garcia-Segura

Keywords:

Photocatalysis
TiO₂/rGO
Dexamethasone
S-metolachlor
Fluoride release
Chloride release

ABSTRACT

This work studies the photocatalytic degradation of solutions containing 0.11 mM of a glucocorticoid (dexamethasone, DEX) and 0.11 mM of an herbicide (S-metolachlor, MTLC), organohalogenated compounds containing fluorine and chlorine atoms in their molecules, respectively. To treat 1 L volume, a mass of 0.5 g of TiO₂/rGO composite in suspension has been used as photocatalyst, irradiated with UV-A LEDs with 200 W m⁻² of irradiance. MTLC is partially adsorbed on the surface of the catalyst, while DEX is not adsorbed, showing different degradation kinetics. The halogen ions released into the solution from the breakage of the parent molecules, F⁻ and Cl⁻ respectively, were analysed. In the case of MTLC, the released Cl⁻ followed two different kinetic trends, being faster, and with a rate that matched the rate of MTLC disappearance, the part corresponding to non-adsorbed MTLC. In the experiments with DEX solutions a different behaviour was observed; the released F⁻ in the photocatalytic degradation was partially adsorbed on the catalyst surface, but the adsorption capacity decreased with the use of the photocatalyst in consecutive cycles until the solubilised F⁻ matched the degraded concentration of DEX. Furthermore, the mass balance between the degraded contaminant and the solubilised halogen anion, for both contaminants, allowed to conclude the absence of halogenated intermediates under the final operating conditions, that is a remarkable outcome in water remediation processes.

* Corresponding author.

E-mail address: ortizi@unican.es (I. Ortiz).

<https://doi.org/10.1016/j.chemosphere.2023.140806>

Received 20 September 2023; Received in revised form 22 November 2023; Accepted 22 November 2023

Available online 29 November 2023

0045-6535/© 2023 The Authors. Published by Elsevier Ltd. This is an open access article under the CC BY-NC-ND license (<http://creativecommons.org/licenses/by-nc-nd/4.0/>).

1. Introduction

As the global population is continuously growing, there is an increasing need to balance the competing demands on water resources. A further consequence of population growth is water pollution. Among water pollutants, halogenated organic compounds (HOCs) present great concern because of their high persistence, potential toxicity or bio-accumulative nature (Munsch et al., 2023; Rivero et al., 2020; Xiuling et al., 2022).

Within the HOCs group, dexamethasone (DEX) (9 α -Fluoro-16 α -methylprednisolone), is a fluorinated glucocorticoid used to treat endocrine, rheumatic, respiratory and other conditions (DrugBank, 2022). DEX has been detected in surface water at concentrations up to 8.78 ng L⁻¹ and can be potentially harmful due to its endocrine disrupting character (Quaresma et al., 2021). Different concentrations of DEX and other glucocorticoid pollutants can be found in hospital effluents, municipal wastewater, and river water within the range of 52–390 ng L⁻¹ (Grilla et al., 2021; Liu et al., 2009; Musee et al., 2021). S-metolachlor (MTLC) (2-chloro-N-(2-ethyl-6-methylphenyl)-N-(1-methoxypropan-2-yl)acetamide) is another hazardous compound detected in water bodies from 0.1 to 10 μ g L⁻¹ (Orge et al., 2017). MTLC is a type of herbicide widely used in crops worldwide (Kouame et al., 2022). In 1993, the World Health Organization (WHO) and the US Environmental Protection Agency listed MTLC as a Class C human carcinogen (Liu et al., 2022). Therefore, both DEX and MTLC are considered contaminants of emerging concern (CECs) (United States Environmental Protection Agency, 2022), so their removal is a global challenge (Espíndola and Vilar, 2020).

Heterogeneous photocatalysis is considered a promising option to eliminate this kind of pollutants in aqueous phase as it is able to fully mineralise the parents compounds thanks to the radicals formed from photoexcited electrons or photoinduced holes, or by direct oxidation by holes on the catalyst surface (Byrne et al., 2018; Hoffmann et al., 1995; Malato et al., 2009; Montenegro-Ayo et al., 2021; Nosaka and Nosaka, 2017; Ollis, 2018; Rizzo et al., 2019; Saravanan et al., 2022; Yadav et al., 2021). Moreover, the ongoing development of LED technology can drastically reduce physical footprint of photocatalytic reactors and their electrical energy requirements (Serrà et al., 2021; Wang et al., 2023). TiO₂ has thoroughly demonstrated its effectiveness as photocatalyst in the degradation of many organic compounds in water. However, to increase the effectiveness of photocatalysis, the strategy of combining TiO₂ with other materials has been widely adopted (Abd Rahman et al., 2023; Lincho et al., 2022; Murgolo et al., 2021). Coupling of reduced graphene oxide (rGO) with semiconductors, in this case TiO₂, offers significant potential to increase the photocatalytic efficiency by providing higher surface area, stability, and fast electron conduction capability (Banerjee et al., 2015; Gómez-Ruiz et al., 2018; Luna-Sanguino et al., 2020; Padmanabhan et al., 2021; Sabir et al., 2021).

Since the photocatalytic degradation of organic substances predominantly takes place on the surface of the photocatalyst, the enrichment of the organic substances close to the photocatalysts is an important contributing factor for achieving higher photocatalytic performance and the adsorption step can play an essential role in the process (Wang et al., 2012; Zhang et al., 2010). Lin et al. (2018) explored the adsorption capacity of TiO₂/rGO composites with 0.5 wt% rGO for degradation of gaseous acetaldehyde and o-xylene. The composite material exhibited a better adsorption for o-xylene owing to the π - π conjugation between rGO and o-xylene. Wang et al. (2013) examined the adsorption ability for phenol on a TiO₂/rGO composite. The adsorption capacity for phenol was improved with the increasing amount of rGO in the composite. Phenol molecules transferred from the solution to the photocatalyst surface via π - π conjugation between phenol and aromatic regions of graphene. Fan et al. (2021b) used TiO₂/rGO with a 0.25 wt% of rGO for phenol adsorption and photocatalysis. They analysed the effect of pH in the solutions and showed that increasing pH did not favour the adsorption of pollutants, thus reducing the efficiency

of photocatalytic degradation. Yu et al. (2016) loaded 1 wt% rGO to TiO₂ for testing the adsorption capacity of the catalyst for two dyes, methyl orange and methylene blue, anionic and cationic dyes, respectively. The presence of the negative rGO nanosheets showed a better adsorption performance for cationic dyes.

In this context, the aim of this work is to assess the individual photocatalytic degradation of DEX and MTLC using TiO₂/rGO with 5% of graphene oxide as photocatalyst focusing on the influence of the adsorption stage complemented with the release of the halogen anions. The stoichiometry of the molecules indicates the absence of halogenated intermediates, and the results of the phytotoxicity tests confirm that the degradation products that remain in solution after treatment are non-toxic. Furthermore, this work reports the performance of photocatalysis after several cycles, analyses the catalyst after use and points to a trade-off between the incorporation of reduced graphene oxide to increase the degradation rate and the usability of the catalyst.

2. Methodology

2.1. Materials

DEX (C₂₂H₂₉FO₅), MTLC (C₁₅H₂₂ClNO₂) PESTANAL® and acetonitrile LiChrosolv® were purchased from Sigma-Aldrich. TiO₂ Aeroxide® P25 was provided by Evonik Degussa. A dispersion of 4 mg mL⁻¹ of graphene oxide (GO) in water was acquired from Graphenea. All standard solutions were prepared in ultrapure water (Milli-Q Millipore system). Polypropylene syringe filters were acquired from Agilent Technologies. All reagents and materials were analytical grade and employed without further treatment.

2.2. Preparation of composite

The photocatalyst, TiO₂/rGO, with a 5% wt. of GO, was prepared following the procedures described in a previous publication (Barquín et al., 2022).

2.3. Photocatalyst characterisation

The UV-Vis-NIR diffuse reflectance spectra were recorded on a spectrophotometer V-770 (Jasco Instruments) with integrating sphere ILN 925 (Jasco Instruments). The surface analysis was studied by X-ray photoelectron spectroscopy (XPS, Kratos AXIS Supra) with a monochromatic Al K α X-ray source at 75 W (5 mA and 15 kV). The high-resolution spectra were energy calibrated by reference to the lowest energy carbon C1s signal at 248.8 eV.

2.4. Photocatalytic activity

The photocatalytic activity was evaluated for the removal of synthetic DEX and MTLC solutions in aqueous phase. The chemical structures of the studied contaminants of emerging concern are shown in Fig. S1 in the supplementary material (SM). Experiments were performed in a 1 L Pyrex glass photoreactor provided with UV-A LED technology purchased from APRIA SYSTEMS, that emitted a fixed wavelength at 365 nm. The reactor housing had 30 LEDs (ENGIN LZ1-00UV00) distributed in 10 strips that were placed at 1.50 cm from the photoreactor. After the adsorption period, the suspension was illuminated with an average irradiance of 200 W m⁻². Irradiance was measured with a Delta Ohm photo/radiometer HD 2102.1 fitted with a UV-A radiation probe. Irradiance was also measured inside the empty glass reactor at three different heights, both in the centre of the reactor and on the reactor wall. The value given is the average of all measurements. Samples were collected, filtered (0.45 μ m), and analysed. Initial concentration of each compounds was 0.11 mM while the catalyst load was 0.5 g L⁻¹.

Both DEX and MTLC concentrations were quantified in a high-performance liquid chromatograph (HPLC) from Agilent, Series 1100, equipped with an Agilent Zorbax 80 Å Extend-C18 column (5 μm , 3.0 \times 150 mm) coupled to a diode array detector (1260 DAD-HS). The injection volume was 50 μL and the column temperature was kept at 30 $^{\circ}\text{C}$. Ultrapure water and acetonitrile were the mobile phases for both compounds, in isocratic mode. For DEX and MTLC, the ratio between the mobile phases were 50/50 and 40/60 with flowrates of 0.5 and 0.7 mL min^{-1} , the retention times were 3.0 and 3.8 min and, finally, the wavelengths were chosen as 240 and 214 nm, respectively. The detection limits were 1.27×10^{-4} and 3.52×10^{-4} mM for DEX and MTLC, respectively.

The released fluoride and chloride to the solution were determined in an ion chromatograph with autosampler, Dionex ICS-5000 using Na_2CO_3 9 mM as mobile phase with an anionic column IonPac AS9-HC (4.0 \times 50 mm) from Thermo Scientific and a flow rate of 1.0 mL min^{-1} . The detection limits were 2.63×10^{-3} and 1.41×10^{-3} mM for F^- and Cl^- , respectively. Every experiment was performed in duplicate, and pH was controlled during the process with a Hanna pHmeter, Edge model.

2.5. Phytotoxicity assessment

The toxicity of the samples was evaluated using the Phytotestkit microbiotest from MicroBioTests Inc. These phytotoxicity assays were performed in agreement with ISO Standard 18763, allowing the evaluation of the germination and growth of three different plant species (*Lepidium sativum*, *Sinapis alba* and *Sorghum saccharatum*). This test is a widely used method to assess the toxicity of aqueous media, regardless the nature of the compound.

The test consisted of germinating the seeds of these mentioned species by adding 20 mL of the previously filtered sample to the test plates and letting them grow for 72 h at 25 $^{\circ}\text{C}$. Control tests were also performed by adding 20 mL of ultrapure water. After that, the number of germinated seeds was determined for the initial, intermediate, and final samples along the photocatalytic treatment, and the length of the roots and stems/shoots was measured. The processing of the results was done using ImageJ software.

3. Results and discussion

3.1. Characterisation

The catalyst characterisation can be found in previous works (Barquín et al., 2022). The band gap of TiO_2/rGO and TiO_2 , for comparison purposes, were estimated from the plots of $(F(R)h\nu)^{1/2}$ versus $h\nu$. The results are shown in Fig. S2 in the SM.

3.2. Photocatalytic activity

Photocatalytic degradation of solutions containing DEX or MTLC with TiO_2/rGO was experimentally assessed under UV-A light irradiation using LED technology. In Fig. 1a, it is evidenced that DEX is not adsorbed onto the catalyst surface and is degraded by photolysis with UV-A light, with a pseudo-first order kinetic constant k of $2.3 \times 10^{-2} \text{ min}^{-1}$. Moreover, the rate of DEX elimination increases more than 5 times with addition of the photocatalyst. Pseudo-first order kinetic constants are shown in Table 1. Other authors have already observed that DEX does not adsorb on TiO_2 -based photocatalysts. Chen et al. (2022) reported that the morphology of TiO_2 has an effect on the adsorption of pollutants. They synthesised TiO_2 flowers with high adsorption capacity and the adsorbed fraction of DEX in the dark after 30 min was negligible, although TiO_2 flowers were capable to adsorb other pollutants such as phenol or Cr (VI).

In the case of MTLC, for the concentration studied in this work, 0.11 mM, photolysis is negligible whereas 50% of the initial pollutant concentration is adsorbed on the photocatalyst at equilibrium in the dark. The adsorption of MTLC on the TiO_2/rGO composite was evaluated in a previous publication and the data were fitted correctly to the Langmuir isotherm, with the maximum adsorption capacity (q_m) being $125.0 \pm 5.4 \text{ mg g}^{-1}$ and the Langmuir's constant (K_{ads}) being $10.1 \times 10^{-3} \pm 3.4 \times 10^{-4} \text{ L mg}^{-1}$ (Barquín et al., 2022). Chen et al. (2007) suggested that the adsorption of organic compounds on multiwalled carbon nanotubes increases with the number of nitro-functional groups. MTLC has one nitrogen atom in its structure and as shown in the photodegradation results, it is highly capable of being adsorbed on the surface of the catalyst. The π electrons in the structure of rGO led to a facile π - π stack with the molecules that contain aromatic groups (Domergue et al., 2022;

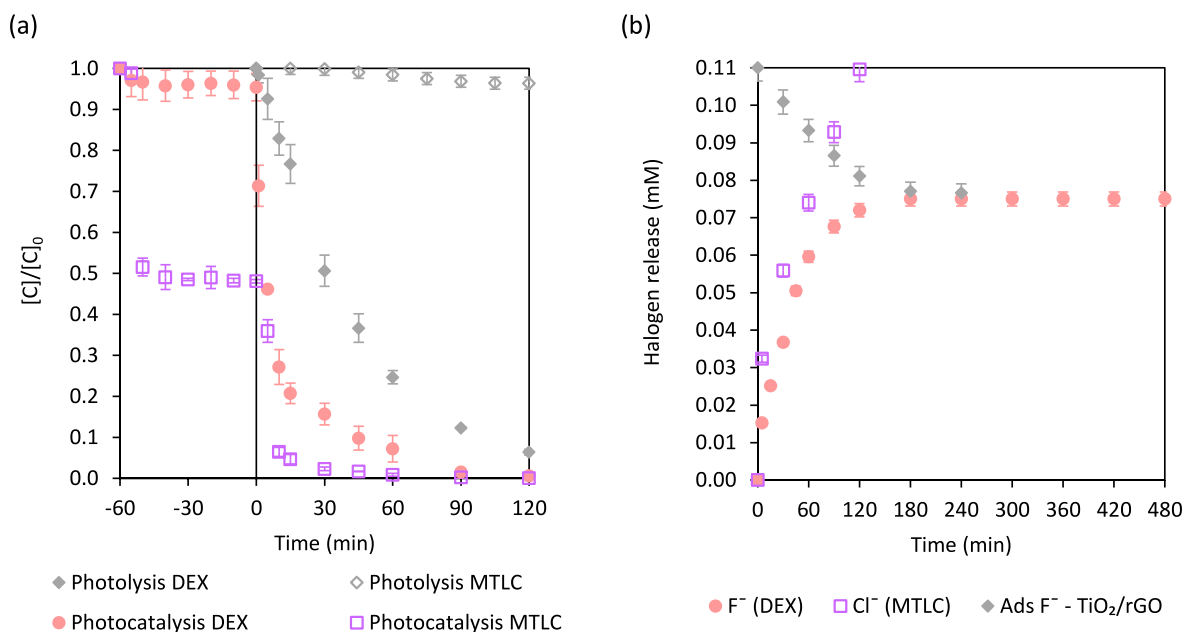


Fig. 1. (a) 0.11 mM DEX and 0.11 mM MTLC removal separately after 120 min of irradiation with UV-A source at 365 nm and (b) halogen release during the experiments.

Table 1

Kinetic constants for the removal of the contaminants and for the halogens released during the photocatalytic experiments.

Photocatalytic removal			Halogen released				
Experiment	k (min ⁻¹)	R ²	Halogen	Fit model	Kinetic constant	Intercept	R ²
Photocatalysis DEX	$(12.8 \pm 0.8) \times 10^{-2}$	0.97	F ⁻	First order	$4.2 \times 10^{-2} \text{ min}^{-1}$	n.a.	0.97
Photocatalysis MTLC	$(16.4 \pm 0.8) \times 10^{-2}$	0.96	Cl ⁻	First order, sol. MTLC	$16.4 \times 10^{-2} \text{ min}^{-1}$	n.a.	0.96
				Zero-th order, ads. MTLC	$0.5 \times 10^{-2} \text{ mM min}^{-1}$	$4.3 \times 10^{-2} \text{ mM}$	0.98

n.a.: not applicable.

Minella et al., 2018; Qin et al., 2014). Also, the reduction of GO to rGO during the synthesis procedure of the photocatalyst improves the hydrophobic character of TiO₂/rGO. In a recent study, Liu et al. (2022) suggested that the main mechanisms responsible for the MTLC adsorption were formation of hydrogen bonds, π - π interactions and hydrophobic forces.

In terms of photocatalytic degradation kinetics, the removal of the dissolved fraction of MTLC can be also represented by a pseudo-first order kinetic model, with a kinetic constant of $16.4 \times 10^{-2} \text{ min}^{-1}$. Adsorption has been widely reported as the premise to photocatalysis; better adsorption of pollutants on the catalyst surface leads to more thorough photocatalytic degradation (Chen et al., 2020, 2022; Xu et al., 2015). For the same initial concentration of both compounds, the adsorption of MTLC is higher than that of DEX; consequently, the remaining concentration in solution is lower when the light is switched on, resulting in a higher degradation kinetic constant of the solubilised fraction of the pollutant. However, as reported by Barquín et al. (2022), the adsorbed MTLC fraction followed a different and slower degradation kinetics as opposed to previous reports; thus, deepening on the role of adsorption on the overall degradation kinetics is still challenging.

Fig. 1b depicts the concentration of the released halogen ions to the aqueous solution as result of the degradation process, fluoride from DEX and chloride from MTLC. It should be noted that since the MTLC molecule contains one nitrogen atom, the possible presence of nitrates and/or nitrites was also investigated by ion chromatography. However, none of these ions were detected, likely because, as reported by Vieira Guelfi et al. (2018), nitrogen is reduced to NH₄⁺; that in the present work would be formed at a very low concentration.

It was previously evidenced that in the MTLC experiments there are two kinetic trends in the chloride release (Barquín et al., 2022), data shown in Table 1. Briefly, when MTLC is dissolved in the aqueous solution, the rate of degradation and chloride release followed both a pseudo-first order kinetics with the same kinetic constant value, $k = 16.4 \times 10^{-2} \text{ min}^{-1}$. After removal of the dissolved fraction of MTLC, the released chloride concentration followed zero-th order kinetics, $k = 0.5 \times 10^{-2} \text{ mM min}^{-1}$. The final chloride concentration after 120 min of irradiation matches the initial chlorine concentration in the MTLC, suggesting that the chloride comes from the adsorbed MTLC and remains in the solution after the complete disappearance of MTLC (Barquín et al., 2022). Regarding DEX experiments, when DEX is totally removed from the solution, the measured fluoride in the solution after 120 min of irradiation is about 70% of the fluorine content in the initial DEX molecules, and its release follows a pseudo-first order kinetics, $k = 4.2 \times 10^{-2} \text{ min}^{-1}$, that is 3 times lower than the rate of DEX photodegradation. These results can be explained by the adsorption of F⁻ on the photocatalyst surface in parallel to its release until the solid becomes saturated, that would lead to a lower presence of fluoride in the solution.

Previous works have reported the adsorption of fluoride ions on different materials such as oxides, carbonaceous materials or industrial products and by-products (Gómez-Ruiz et al., 2018; Habuda-Stanić et al., 2014; Nehra et al., 2019; Suriyaraj et al., 2014). DEX experiments started at pH \approx 6 and ended at pH \approx 4, always under acidic conditions. The isoelectric point for TiO₂/rGO was experimentally obtained at pH \approx 5.8 (Barquín et al., 2022). At pH values below 5.8, the photocatalyst is positively charged and attracts the negatively charged fluoride ion. As soon as the catalyst is in contact with the DEX solution, the pH decreases

from \approx 6 to \approx 4.9, when the catalyst is positively charged and the adsorption of F⁻ is promoted. To furthermore confirm that the fluoride released into the solution is being adsorbed on the catalyst, 0.11 mM of F⁻ (from fluoride standard for IC, TraceCERT®) were contacted with 0.5 g L⁻¹ of TiO₂/rGO, results shown in Fig. 1b. In the first 180 min, F⁻ concentration in the solution decreased by 30%, and afterwards the concentration remained constant, indicating a possible saturation of the catalyst surface. In summary, with the values obtained by ion chromatography, it can be calculated that the sum of the F⁻ released to the solution, 0.077 mM, and the F⁻ adsorbed on the catalyst surface, 0.033 mM, corresponded to the initial fluorine content in the DEX molecules, 0.11 mM. Table 1 collects the values of the kinetic constants corresponding to the release of anions.

Regarding halogen ions, it is also important to understand how they are released into the solution. For DEX, it is common for the C-F bond to be broken in the first stage of its photodegradation. DEX loses the fluorine atom by reductive dehalogenation (Calza et al., 2001; Pazoki et al., 2016; Pretali et al., 2021; Rasolevandi et al., 2019). For MTLC, Mermana et al. (2017) proposed that the dechlorination of MTLC can occur i) by displacement of chloride by a nucleophilic superoxide radical or ii) by the abstraction of a benzylic hydrogen atom by hydroxyl radical or superoxide anion radical, leading to the formation of a cyclic product. Also, Chusaksri et al. (2011) evidenced that chloride is formed at the early stage of the oxidation. Scheme S1 and scheme S2 in SM depict the aforementioned dehalogenation mechanisms for DEX and MTLC, respectively.

3.3. Catalyst reuse

The reusability of the photocatalysts plays a significant role in water remediation processes. Hence, five reusability experiments, 120 min each, of each pollutant were carried out with the same photocatalyst, Fig. 2. After every cycle, the catalyst was centrifuged at 10000 rpm for 3 min and used for the next cycle by keeping constant the rest of operating conditions.

Both DEX and MTLC are still removed after five cycles using 0.5 g L⁻¹ of TiO₂/rGO. Nevertheless, the initial degradation rates decrease after every cycle. Table 2 shows that in all experiments, the kinetic constant decreases cycle by cycle. In the case of DEX, the kinetic constant in the first cycle is $12.8 \times 10^{-2} \text{ min}^{-1}$ while in the fifth cycle the kinetic constant is reduced by 33%. For MTLC experiments, kinetic constants vary from $16.4 \times 10^{-2} \text{ min}^{-1}$ in the first cycle to $9.2 \times 10^{-2} \text{ min}^{-1}$ in the last cycle, which represents a 44% decrease. The reduction in the degradation kinetic constants of both compounds is not only due to the associated mass loss in each cycle. To avoid the influence of the loss of catalyst mass during the sampling procedure and centrifugation stage on the kinetic data, the initial degradation rates were compared, Table 2. In DEX experiments, the first degradation rate is $11.5 \times 10^{-3} \text{ mmol min}^{-1} \text{ g}_{\text{cat}}^{-1}$ while in the fifth cycle the degradation rate is reduced by 43%. For MTLC experiments, the first degradation rate is $6.1 \times 10^{-3} \text{ mmol min}^{-1} \text{ g}_{\text{cat}}^{-1}$ while in the fifth cycle there is a drop of 38%. Nevertheless, a catalyst deactivation is observed.

Fig. 2a represents in bars the fluoride released from DEX molecules in each cycle. During the first run, 70% of the total F⁻ was released after 120 min of irradiation. Fig. 3 plots the mass balance between the degraded DEX and the measured F⁻ in the solution over the 5 cycles. The

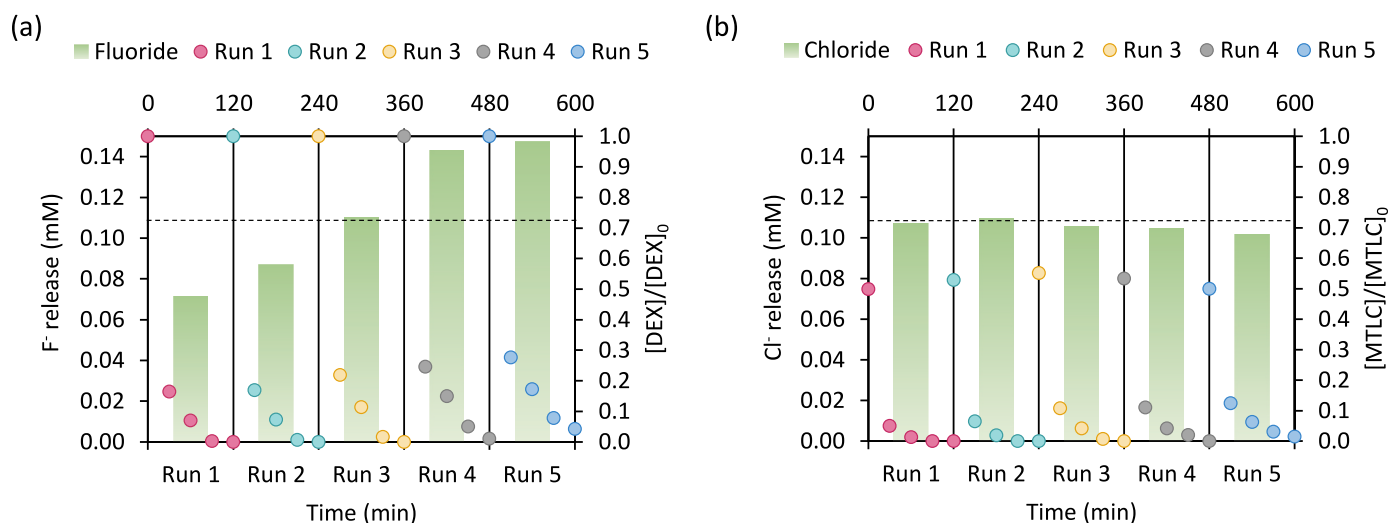


Fig. 2. TiO_2/rGO reusability studies for (a) DEX and (b) MTLC experiments.

Table 2

Pseudo-first order kinetic constants and initial degradation rates for five consecutive cycles performed with DEX and MTLC.

Run	DEX			MTLC			DEX		
	TiO_2/rGO (g L^{-1})	k (min^{-1})	r_0 ($\text{mmol min}^{-1} \text{g}_{\text{cat}}^{-1}$)	TiO_2/rGO (g L^{-1})	k (min^{-1})	r_0 ($\text{mmol min}^{-1} \text{g}_{\text{cat}}^{-1}$)	TiO_2 (g L^{-1})	k (min^{-1})	r_0 ($\text{mmol min}^{-1} \text{g}_{\text{cat}}^{-1}$)
1	0.50	12.8×10^{-2}	11.5×10^{-3}	0.50	16.4×10^{-2}	6.1×10^{-3}	0.50	6.8×10^{-2}	4.0×10^{-3}
2	0.48	11.8×10^{-2}	10.7×10^{-3}	0.48	14.0×10^{-2}	6.0×10^{-3}	0.47	6.3×10^{-2}	3.7×10^{-3}
3	0.46	10.1×10^{-2}	9.2×10^{-3}	0.46	10.9×10^{-2}	5.2×10^{-3}	0.44	6.0×10^{-2}	4.1×10^{-3}
4	0.45	9.4×10^{-2}	8.1×10^{-3}	0.44	10.5×10^{-2}	4.7×10^{-3}	0.41	5.7×10^{-2}	3.6×10^{-3}
5	0.43	8.6×10^{-2}	6.6×10^{-3}	0.42	9.2×10^{-2}	3.8×10^{-3}	0.37	5.4×10^{-2}	3.9×10^{-3}

“accumulated DEX degraded” represents the sum of the amount of DEX removed in each cycle. On the other hand, the “accumulated F^- released” is the sum of the fluoride released into the solution in each of the 5 cycles, quantified by ion chromatography. The molar ratio between DEX and fluoride is 1:1; so, for each mole of DEX removed, 1 mol of F^- can be expected to be released if no intermediate fluorinated

compounds remain in solution. If this ratio is fulfilled, then the experimental data should coincide with the bisector of Fig. 3, represented by the black line. The grey lines in Fig. 3 represent the zone with error of $\pm 10\%$ around the bisector. In Fig. 3 it can be observed a very good match that underscores the absence of halogenated intermediates under the final operation conditions when TiO_2/rGO is used as photocatalyst.

In Fig. 3, experimental data evidence that the degradation of DEX takes place through the breakage of the fluorine bond releasing F^- to the solution.

In the case of MTLC, the chloride released is depicted in Fig. 2b. The tendency is similar in all the cycles with a slight reduction in the chloride concentration in solution parallel to the reduction in the degradation rate of MTLC. Overall, the concentration of released chloride matched the initial chlorine content in the MTLC molecules. Therefore, these results indicate that no organohalogenated intermediates remained in solution after the photocatalytic treatment, at least in quantifiable concentration. Moreover, in DEX experiments it is noteworthy that the decrease in the degradation rate with successive cycles is slightly higher than in MTLC experiments, which could be affected by the negative influence of the presence (and adsorption tendency on the photocatalyst surface) of the released fluoride in the solution.

XPS analysis, Fig. 4, was used to confirm the presence of adsorbed fluoride in the catalyst. The XPS spectra of the TiO_2/rGO were examined before and after being used with DEX or MTLC.

In the XPS whole spectra of the different samples, Fig. 4a, the peaks of the components have no significant change in the spectral shape, which indicates that the photocatalyst maintains its crystal structure after being used in the experiments. In Fig. 4b the deconvoluted spectra of C1s is depicted. In all samples, the peak with a binding energy (BE) of 284.80 eV can be attributed to the C–C, C=C, and C–H bonds, and this peak is used for fixing the reference energy (Wang and Zhang, 2011). Then, ~ 0.92 , ~ 2.19 , ~ 4.8 eV above the reference in terms of the BE can be associated to the C–O, C=O and O=C–OH functional groups,

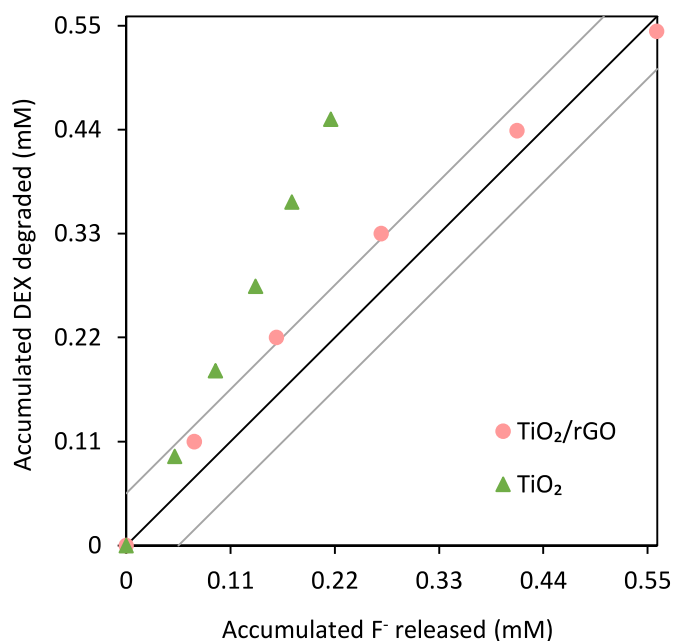


Fig. 3. Mass balance of accumulated DEX degraded in five consecutive cycles and the corresponding fluoride released in solution for TiO_2 and TiO_2/rGO .

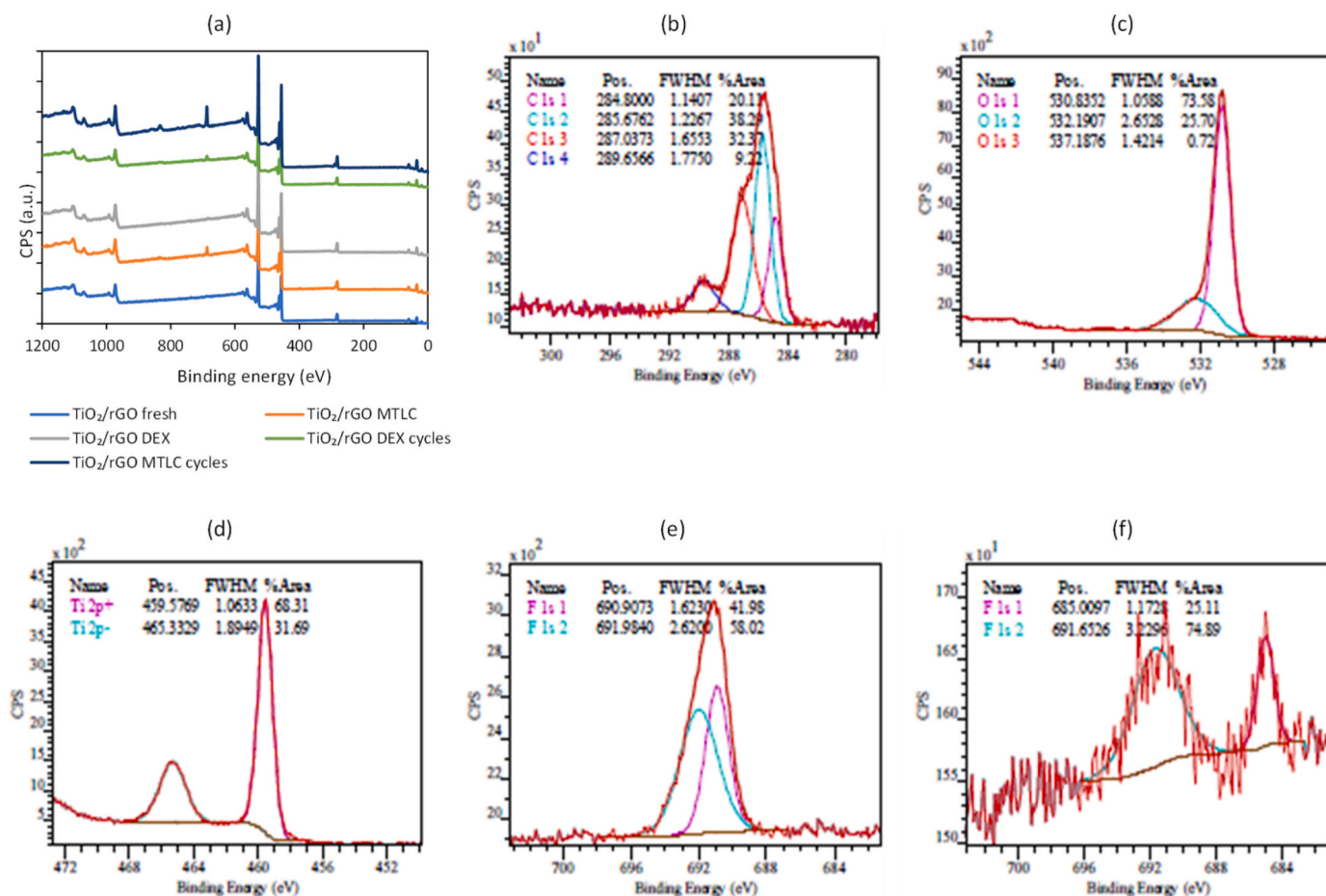


Fig. 4. XPS survey (a) and XPS peak deconvolution of the binding energy regions of: C1s of TiO₂/rGO fresh (b), O1s of TiO₂/rGO fresh (c), Ti2p of TiO₂/rGO fresh (d), F1s of TiO₂/rGO used with DEX after 1 cycle (e), and F1s of TiO₂/rGO used with DEX after 5 cycles (f).

respectively (Briggs and Seah, 1990; Wang and Zhang, 2011). The presence of these bonds demonstrates that GO was reduced to rGO during the composite synthesis and specially the C=C bond improves the conductivity of the catalyst, which is important for the efficient electron transfer (Fan et al., 2021a; Lin et al., 2018). The XPS peak deconvolution of the O1s region, Fig. 4c, mainly consists of two components; the first one at BE~530 eV assigned to O in TiO₂ (Karaolia et al., 2018), and the second one, which has a higher BE by 1–2 eV assigned to hydroxyls, carboxyls or adsorbed water (Karaolia et al., 2018; McCafferty and Wightman, 1998). Regarding Ti2p spectra, Fig. 4d, no changes in the titanium structure when analysing the results of used and fresh catalysts, indicating that catalysts retain its electronic structure. The two main peaks located at 459.58 eV and 465.34 eV can be attributed to Ti2p_{3/2} and Ti2p_{1/2} respectively. In addition, the splitting between both peaks is 5.7 eV, which indicates a Ti(IV) chemical state, typical of TiO₂ in GO-TiO₂ composites (Benjwal et al., 2015; Pastrana-Martínez et al., 2012). Ti2p spectrum corresponds to the TiO₂ commercial sample, showing symmetric components 2p_{3/2} and 2p_{1/2} (ThermoScientific Knowledge Database, n.d.). Finally, in Fig. 4e and f the deconvolutions of the binding energy region of F1s are depicted for the composite used with DEX after 1 and 5 cycles, respectively. This peak, located at 690.56 eV, is observed in the sample after 1 cycle, indicating that F⁻ is adsorbed on the catalyst surface after being used. However, after 5 cycles, the presence of fluorine on the catalyst is negligible, as can be seen in Fig. 4f. This is an indication that no fluorine remains adsorbed on the surface of the catalyst after several cycles.

Additionally, to gain insight on the role of fluoride adsorption on TiO₂-based photocatalysts, experiments of DEX photodegradation with

0.5 g L⁻¹ of commercial TiO₂ P25 were carried out. Five consecutive cycles of DEX degradation were performed, Fig. 5.

The results in Fig. 5 indicate that TiO₂ P25 does not achieve complete degradation of DEX after 120 min of light in any of the cycles. On average, 19% of the initial DEX concentration remains in solution. The catalyst recovery was more difficult than the composite, and more mass was lost during these experiments. Looking at the pseudo-first order

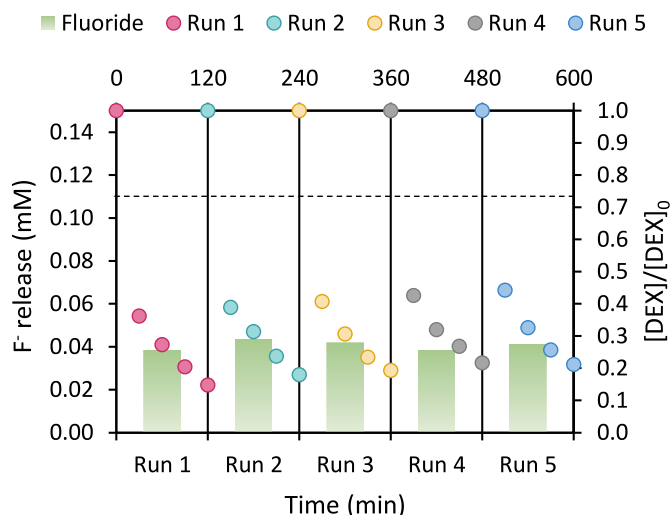


Fig. 5. TiO₂ reusability studies for DEX experiments.

kinetic constants of DEX degradation with commercial TiO_2 over the cycles, shown in Table 2, the values decrease in each cycle and after the fifth cycle a deactivation of 20% is appreciated. Regarding the initial degradation rates of Table 2 for DEX experiments with TiO_2 , all cycles are in the same range of values, $3.9 \times 10^{-3} \pm 0.2 \times 10^{-3} \text{ mmol min}^{-1} \text{ g}_{\text{cat}}^{-1}$, however, when comparing the first and fifth cycles, the degradation of DEX after 120 min, falls down from 85% to 79%. The concentration of fluoride in the medium remained practically constant around 0.04 mM, corresponding to 36.4% of the initial fluorine in DEX molecules. In the experiments focused on the reuse of TiO_2 , the difference between the theoretical fluoride corresponding to the degraded DEX and the measured fluoride in solution is 0.05 mM, which is higher than the difference in the case of the composite. In order to clarify whether this difference could be attributed to the adsorption of F^- on TiO_2 or to the presence of halogenated intermediates, commercial TiO_2 was also tested for fluoride adsorption from a solution containing 0.11 mM of F^- and 0.5 g L^{-1} of TiO_2 P25. After 30 min of contact, the adsorption equilibrium of fluoride was reached, being the amount of fluoride adsorbed on TiO_2 12% of the initial value, which corresponds to $\approx 0.01 \text{ mM}$. The obtained results in absence or presence of UV-A light were similar. This finding agreed with previous observation of Suriyaraj et al. (2014), who showed that all phases of TiO_2 have the ability to adsorb F^- , and in particular the adsorption of F^- in the catalyst increases when the percentage of anatase phase is increased. It was experimentally observed that the adsorption of F^- on commercial TiO_2 is lower than on the composite. Therefore, these results confirm i) that the presence of 5% GO in the catalyst increases the adsorption of F^- on the composite with respect to commercial TiO_2 and ii) the likely presence of halogenated intermediates in the aqueous medium when TiO_2 is used as photocatalyst.

The mass balance between the accumulated degraded DEX and the fluoride released in each cycle is shown in Fig. 3 for the composite and for commercial TiO_2 . When TiO_2/rGO is used as photocatalyst, the mass balance evidences that for both contaminants all the halogenated atoms in the parent compound are released in solution, thus, allowing to conclude that under these operational conditions there are no halogenated intermediates in quantifiable concentrations. In the photocatalytic degradation of DEX, there is more fluoride in solution when using the composite TiO_2/rGO than with bare TiO_2 , which is consistent with the faster degradation rate of the contaminant with the composite photocatalyst. Fig. 3 shows that in the case of TiO_2/rGO , the experimental match between the moles of degraded DEX and the moles of released fluoride are within the 10% error. This finding is not observed for TiO_2 P25. In the case of TiO_2 , the results deviate from the bisector because there are more moles of degraded DEX than of released fluoride, thus pointing to the likely presence of organofluorinated intermediates in the aqueous medium. Therefore, given the relevance of this finding, this is an objective for ongoing research.

Additionally, the pseudo-first order kinetic constants shown in Table 2, indicate that with the composite are between 2.0 and 1.6 times higher than with TiO_2 , suggesting that the reduced graphene oxide promotes the electron transfer rate and enhances the photocatalytic activity. These values agree with previous literature reports; Lu et al. (2021) reported that the incorporation of rGO into photocatalysts boosts the photocatalytic activity by 1.3–10 times compared to the same photocatalysts without rGO (Lu et al., 2021). It is well established in the literature that the presence of rGO efficiently suppresses the recombination of photogenerated electron-hole pairs and facilitates the transfer of photogenerated electrons from the conduction bands of semiconductors to the graphene sheets (Cruz et al., 2017; Koli et al., 2022; Mondal et al., 2021; Pérez-Molina et al., 2020; Xu et al., 2018; Zhao et al., 2017).

In general, there is a lack of knowledge regarding the deactivation of photocatalysts. Cheng et al. (2016) synthesised a composite material consisting of gold nanoparticles supported on layered TiO_2/rGO for microwave-assisted hydration reaction of phenylacetylene. They

performed some cycles with the same photocatalyst, recovered by filtration or centrifugation, and they attributed the decrease in activity to the loss of active sites of the catalyst. With nanocomposites based on TiO_2 , rGO and Pt, Esteves et al. (2021) photogenerated hydrogen from ethanol liquid and gas phases. The presence of a 3% of rGO reinforced the effect of Pt as suppressor of charge recombination. However, for a higher rGO content there was a decrease in the hydrogen generation rate, that was attributed to a higher absorption of radiation by rGO and consequently a lesser absorption by TiO_2 . In the photodegradation of VOCs, Rao et al. (2021) introduced Er^{3+} in a composite formed of TiO_2 and rGO. The presence of the rare earth substantially improved the photogenerated electron-hole pair separation, resulting in high photocatalytic activity. In that case, rGO played a vital role in keeping the stable activity of the composites. They claimed that catalyst deactivation was caused by the accumulation of intermediates on the photocatalyst surface.

3.4. Phytotoxicity assessment

When oxidation takes place, reaction intermediates and final oxidation products may become more hazardous than the parent compounds (García-Costa et al., 2022; Zazo et al., 2007). Therefore, phytotoxicity tests were performed using three different species (*Lepidium sativum* (LES), *Sinapis alba* (SIA) and *Sorghum saccharatum* (SOS)).

Fig. S3 collects the measurements of the roots and shoots, expressed in mm, of the three seeds during the photocatalytic process, as well as the measurements of the control sample (20 mL of ultrapure water). In addition, ultrapure water was contacted with TiO_2/rGO , 60 min in the absence of light and then 120 min with UV-A light, to know if the catalyst has any effect on the toxicity of the samples. Mainly, after the whole photocatalytic treatment of 480 min of UV-A irradiation light, nor DEX samples or MTLC samples show signs of toxicity, all values exceed the control. Considering that: i) no halogenated compounds remain in solution and, ii) knowing from toxicity tests that the compounds remaining in solution are not toxic, it can be concluded that photocatalysis with TiO_2/rGO is a good technology for the removal of DEX and MTLC.

4. Conclusions

In this work, TiO_2/rGO composites were prepared by hydrothermal method and used as effective photocatalysts for the removal of two HOCs, DEX and MTLC, which showed a different adsorption pattern on the photocatalyst surface. Whereas the chlorinated MTLC was partially adsorbed on the photocatalyst and consequently followed two different degradation kinetics, being slower the degradation of the adsorbed part; the fluorinated DEX was not adsorbed. However, the fluoride released from the breakage of the DEX molecule was partially adsorbed on the photocatalyst surface, as confirmed by XPS analysis. The results of photodegradation consecutive cycles evidenced a loss of photocatalytic activity that in the case of DEX photodegradation was accompanied with the increased concentration of F^- in the solution; this observation pointed to a change of the photocatalyst surface and properties, that needs further research. The mass balance between the degraded contaminant and the solubilised halogen after 5 consecutive cycles allowed to conclude the absence of halogenated intermediates in the solution, fact that is of high relevance for the implementation of the technology. Besides, the phytotoxicity test, in accordance with ISO Standard 18763, confirmed that after 480 min of UV-A light irradiation, the final samples are non-toxic. Finally, the comparison of photodegradation results with the composite and with commercial TiO_2 clarified that the presence of rGO significantly improved the degradation rate of halogenated compounds. For future work, it is proposed to investigate the behaviour of the two contaminants of emerging concern when mixed in the same solution.

CRediT authorship contribution statement

Carmen Barquín: Formal analysis, Investigation, Methodology, Validation, Writing - original draft, Writing - review & editing. **María J. Rivero:** Conceptualization, Funding acquisition, Methodology, Project administration, Resources, Supervision, Validation, Writing - review & editing. **Inmaculada Ortiz:** Conceptualization, Funding acquisition, Methodology, Resources, Supervision, Validation, Writing - review & editing.

Declaration of competing interest

The authors declare that they have no known competing financial interests or personal relationships that could have appeared to influence the work reported in this paper.

Data availability

The data that has been used is confidential.

Acknowledgements

These results are part of the R&D projects PID2021-122563OB-I00 funded by MCIN/AEI/10.13039/501100011033 and “ERDF A way of making Europe” and PDC2022-133563-I00, funded by MCIN/AEI/10.13039/501100011033 and “UE Next Generation EU/PRTR”. Carmen Barquín is also grateful for the FPI contract PRE2019-089096.

Appendix A. Supplementary data

Supplementary data to this article can be found online at <https://doi.org/10.1016/j.chemosphere.2023.140806>.

References

- Abd Rahman, N., Choong, C.E., Pichiah, S., Nah, I.W., Kim, J.R., Oh, S.E., Yoon, Y., Choi, E.H., Jang, M., 2023. Recent advances in the TiO₂ based photoreactors for removing contaminants of emerging concern in water. *Sep. Purif. Technol.* 304, 122294 <https://doi.org/10.1016/j.seppur.2022.122294>.
- Banerjee, S., Dionysiou, D.D., Pillai, S.C., 2015. Self-cleaning applications of TiO₂ by photo-induced hydrophilicity and photocatalysis. *Appl. Catal. B Environ.* 176–177, 396–428. <https://doi.org/10.1016/j.apcatb.2015.03.058>.
- Barquín, C., Rivero, M.J., Ortiz, I., 2022. Shedding light on the performance of magnetically recoverable TiO₂/Fe₃O₄/rGO-5 photocatalyst. Degradation of S-metolachlor as case study. *Chemosphere* 307, 135991. <https://doi.org/10.1016/j.chemosphere.2022.135991>.
- Benjwal, P., Kumar, M., Chamoli, P., Kar, K.K., 2015. Enhanced photocatalytic degradation of methylene blue and adsorption of arsenic(III) by reduced graphene oxide (rGO)-metal oxide (TiO₂/Fe₃O₄) based nanocomposites. *RSC Adv.* 5, 73249 <https://doi.org/10.1039/c5ra13689j>.
- Briggs, D., Seah, M.P., 1990. *Practical surface analysis. In: Auger and X-Ray Photoelectron Spectroscopy*, second ed., vol. 1. John Wiley & Sons. 1990.
- Byrne, C., Subramanian, G., Pillai, S.C., 2018. Recent advances in photocatalysis for environmental applications. *J. Environ. Chem. Eng.* 6, 3531–3555. <https://doi.org/10.1016/j.jece.2017.07.080>.
- Calza, P., Pelizzetti, E., Brüssino, M., Baiocchi, C., 2001. Ion trap tandem mass spectrometry study of dexamethasone transformation products on light activated TiO₂ surface. *J. Am. Soc. Mass Spectrom.* 12, 1286–1295. [https://doi.org/10.1016/S1044-0305\(01\)00319-1](https://doi.org/10.1016/S1044-0305(01)00319-1).
- Chen, W., Duan, L., Zhu, D., 2007. Adsorption of polar and nonpolar organic chemicals to carbon nanotubes. *Environ. Sci. Technol.* 41, 8295–8300. <https://doi.org/10.1021/es071230h>.
- Chen, Y., Zhang, X., Wang, L., Cheng, X., Shang, Q., 2020. Rapid removal of phenol/antibiotics in water by Fe-(8-hydroxyquinoline-7-carboxylic)/TiO₂ flower composite: adsorption combined with photocatalysis. *Chem. Eng. J.* 402 <https://doi.org/10.1016/j.cej.2020.126260>.
- Chen, Y., Yang, L., Sun, Y., Guan, R., Liu, D., Zhao, J., Shang, Q., 2022. A high-performance composite CDs@Cu-HQCA/TiO₂ flower photocatalyst: synergy of complex-sensitization, TiO₂-morphology control and carbon dot-surface modification. *Chem. Eng. J.* 436, 134978 <https://doi.org/10.1016/j.cej.2022.134978>.
- Cheng, Y., Zhao, Q., Li, Y., Peng, W., Zhang, G., Zhang, F., Fan, X., 2016. Gold nanoparticles supported on layered TiO₂-RGO hybrid as an enhanced and recyclable catalyst for microwave-assisted hydration reaction. *RSC Adv.* 6, 76151–76157. <https://doi.org/10.1039/c6ra08021a>.
- Chusaksri, S., Lomda, J., Saleepochn, T., Sutthivaiyakit, P., 2011. Photocatalytic degradation of 3,4-dichlorophenylurea in aqueous gold nanoparticles-modified titanium dioxide suspension under simulated solar light. *J. Hazard Mater.* 190, 930–937. <https://doi.org/10.1016/j.jhazmat.2011.04.028>.
- Cruz, M., Gomez, C., Duran-Valle, C.J., Pastrana-Martínez, L.M., Faria, J.L., Silva, A.M.T., Faraldos, M., Bahamonde, A., 2017. Bare TiO₂ and graphene oxide TiO₂ photocatalysts on the degradation of selected pesticides and influence of the water matrix. *Appl. Surf. Sci.* 416, 1013–1021. <https://doi.org/10.1016/j.apusc.2015.09.268>.
- Domergue, L., Cimetière, N., Giraudet, S., Cloirec, P. Le, 2022. Adsorption onto granular activated carbons of a mixture of pesticides and their metabolites at trace concentrations in groundwater. *J. Environ. Chem. Eng.* 10 <https://doi.org/10.1016/j.jece.2022.108218>.
- DrugBank, 2022. Dexamethasone. <https://go.drugbank.com/drugs/DB011234>, 12.2.22.
- Espindola, J.C., Vilar, V.J.P., 2020. Innovative light-driven chemical/catalytic reactors towards contaminants of emerging concern mitigation: a review. *Chem. Eng. J.* 394, 124865 <https://doi.org/10.1016/j.cej.2020.124865>.
- Esteves, M.A., Fresno, F., Fernandes, V.R., Oropeza, F.E., De, V.A., 2021. TiO₂-reduced graphene oxide-Pt nanocomposites for the photogeneration of hydrogen from ethanol liquid and gas phases. *Catal. Today.* <https://doi.org/10.1016/j.cattod.2021.05.012>.
- Fan, H., Yi, G., Zhang, X., Xing, B., Zhang, C., Chen, L., Zhang, Y., 2021a. Facile synthesis of uniformly loaded Fe₃O₄-TiO₂/RGO ternary hybrids for enhanced photocatalytic activities. *Opt. Mater.* 111, 110582 <https://doi.org/10.1016/j.optmat.2020.110582>.
- Fan, H., Yi, G., Zhang, Z., Zhang, X., Li, P., Zhang, C., Chen, L., Zhang, Y., Sun, Q., 2021b. Binary TiO₂/RGO photocatalyst for enhanced degradation of phenol and its application in underground coal gasification wastewater treatment. *Opt. Mater.* 120, 111482 <https://doi.org/10.1016/j.optmat.2021.111482>.
- Garcia-Costa, A.L., Gouveia, T.I.A., Pereira, M.F.R., Silva, A.M.T., Madeira, L.M., Alves, A., Santos, M.S.F., 2022. Intensification strategies for cytostatics degradation by ozone-based processes in aqueous phase. *J. Hazard Mater.* 440 <https://doi.org/10.1016/j.jhazmat.2022.129743>.
- Gómez-Ruiz, B., Ribao, P., Diban, N., Rivero, M.J., Ortiz, I., Urriaga, A., 2018. Photocatalytic degradation and mineralization of perfluorooctanoic acid (PFOA) using a composite TiO₂-rGO catalyst. *J. Hazard Mater.* 344, 950–957. <https://doi.org/10.1016/j.jhazmat.2017.11.048>.
- Grilla, E., Taheri, M.E., Miserli, K., Venieri, D., Konstantinou, I., Mantzavinos, D., 2021. Degradation of dexamethasone in water using BDD anodic oxidation and persulfate: reaction kinetics and pathways. *J. Chem. Technol. Biotechnol.* 96, 2451–2460. <https://doi.org/10.1002/jctb.6833>.
- Habuda-Stanić, M., Ravancić, M., Flanagan, A., 2014. A review on adsorption of fluoride from aqueous solution. *Materials* 7, 6317–6366. <https://doi.org/10.3390/ma7096317>.
- Hoffmann, M.R., Martin, S.T., Choi, W., Bahnemann, D.W., 1995. Environmental applications of semiconductor photocatalysis. *Chem. Rev.* 95, 69–96. <https://doi.org/10.1021/cr00033a004>.
- Karaolia, P., Michael-Kordatou, I., Hapeshi, E., Drosou, C., Bertakis, Y., Christofilos, D., Armatas, G.S., Sygellou, L., Schwartz, T., Xekoukoulotakis, N.P., Fatta-Kassinos, D., 2018. Removal of antibiotics, antibiotic-resistant bacteria and their associated genes by graphene-based TiO₂ composite photocatalysts under solar radiation in urban wastewaters. *Appl. Catal. B Environ.* 224, 810–824. <https://doi.org/10.1016/j.apcatb.2017.11.020>.
- Koli, V.B., Ragesh Nath, R., Chen, J.R., Ke, S.C., 2022. Enhanced photocatalytic inactivation of bacteria and degradation of pharmaceutical pollutant by rGO/N-TiO₂ nanocomposites: a study of active radicals. *J. Nanoparticle Res.* 24, 1–20. <https://doi.org/10.1007/s11051-022-05538-9>.
- Kouame, K.B.-J., Savin, M.C., Willett, C.D., Bertucci, M.B., Butts, T.R., Grantz, E., Roma-Burgos, N., 2022. S-metolachlor persistence in soil as influenced by within-season and inter-annual herbicide use. *Environ. Adv.* 9, 100318 <https://doi.org/10.1016/j.envadv.2022.100318>.
- Lin, W., Xie, X., Wang, X., Wang, Y., Segets, D., Sun, J., 2018. Efficient adsorption and sustainable degradation of gaseous acetaldehyde and o-xylene using rGO-TiO₂ photocatalyst. *Chem. Eng. J.* 349, 708–718. <https://doi.org/10.1016/j.cej.2018.05.107>.
- Lincho, J., Zaleska-Medynska, A., Martins, R.C., Gomes, J., 2022. Nanostructured photocatalysts for the abatement of contaminants by photocatalysis and photocatalytic ozonation: an overview. *Sci. Total Environ.* 837 <https://doi.org/10.1016/j.scitotenv.2022.155776>.
- Liu, L., Li, X., Wang, X., Wang, Y., Shao, Z., Liu, X., Shan, D., Liu, Z., Dai, Y., 2022. Metolachlor adsorption using walnut shell biochar modified by soil minerals. *Environ. Pollut.* 308, 119610 <https://doi.org/10.1016/j.envpol.2022.119610>.
- Liu, Z., hua, Kanjo, Y., Mizutani, S., 2009. Removal mechanisms for endocrine disrupting compounds (EDCs) in wastewater treatment - physical means, biodegradation, and chemical advanced oxidation: a review. *Sci. Total Environ.* 407, 731–748. <https://doi.org/10.1016/j.scitotenv.2008.08.039>.
- Lu, K.Q., Li, Y.H., Tang, Z.R., Xu, Y.J., 2021. Roles of graphene oxide in heterogeneous photocatalysis. *ACS Mater. Au* 1, 37–54. <https://doi.org/10.1021/acsmaterialsau.1c00022>.
- Luna-Sanguino, G., Ruíz-Delgado, A., Tolosana-Moranchel, A., Pascual, L., Malato, S., Bahamonde, A., Faraldos, M., 2020. Solar photocatalytic degradation of pesticides over TiO₂-rGO nanocomposites at pilot plant scale. *Sci. Total Environ.* 737, 140286 <https://doi.org/10.1016/j.scitotenv.2020.140286>.
- Malato, S., Fernández-Ibáñez, P., Maldonado, M.I., Blanco, J., Gernjak, W., 2009. Decontamination and disinfection of water by solar photocatalysis: recent overview and trends. *Catal. Today* 147, 1–59. <https://doi.org/10.1016/j.cattod.2009.06.018>.

- McCafferty, E., Wightman, J.P., 1998. Determination of the concentration of surface hydroxyl groups on metal oxide films by a quantitative XPS method. *Surf. Interface Anal.* 26, 199807 [https://doi.org/10.1002/\(sici\)1096-9918](https://doi.org/10.1002/(sici)1096-9918), 549 26:8<549>;aid-sia396>3.3.co;2-h.
- Mermaña, J., Suthivaiyakit, P., Blaise, C., Gagné, F., Charnsethikul, S., Kidkhunthod, P., Suthivaiyakit, S., 2017. Photocatalysis of S-metolachlor in aqueous suspension of magnetic cerium-doped TiO_2 core-shell under simulated solar light. *Environ. Sci. Pollut. Res.* 24, 4077–4092. <https://doi.org/10.1007/s11356-016-8151-6>.
- Minella, M., Bertaina, F., Minero, C., 2018. The complex interplay between adsorption and photoactivity in hybrids rGO/ TiO_2 . *Catal. Today* 315, 9–18. <https://doi.org/10.1016/j.cattod.2018.03.026>.
- Mondal, A., Prabhakaran, A., Gupta, S., Subramanian, V.R., 2021. Boosting photocatalytic activity using reduced graphene oxide (RGO)/Semiconductor nanocomposites: issues and future scope. *ACS Omega* 6, 8734–8743. <https://doi.org/10.1021/acsomega.0c06045>.
- Montenegro-Ayo, R., Morales-Gomero, J.C., Alarcon, H., Corzo, A., Westerhoff, P., Garcia-Segura, S., 2021. Photoelectrocatalytic degradation of 2,4-dichlorophenol in a TiO_2 nanotube-coated disc flow reactor. *Chemosphere* 268. <https://doi.org/10.1016/j.chemosphere.2020.129320>.
- Munsch, C., Bely, N., Héas-Moisán, K., Olivier, N., Pollono, C., Govinden, R., Bodin, N., 2023. Species-specific bioaccumulation of persistent organohalogen contaminants in a tropical marine ecosystem (Seychelles, western Indian Ocean). *Chemosphere* 336. <https://doi.org/10.1016/j.chemosphere.2023.139307>.
- Murgolo, S., De Ceglie, C., Di Iaconi, C., Mascolo, G., 2021. Novel TiO_2 -based catalysts employed in photocatalysis and photoelectrocatalysis for effective degradation of pharmaceuticals (PhACs) in water: a short review. *Curr. Opin. Green Sustain. Chem.* 30, 100473 <https://doi.org/10.1016/j.cogsc.2021.100473>.
- Musee, N., Kebaabetswe, L.P., Tichapondwa, S., Tubatsi, G., Mahaye, N., Leareng, S.K., Nomngongo, P.N., 2021. Occurrence, fate, effects, and risks of dexamethasone: ecological implications post-covid-19. *Int. J. Environ. Res. Publ. Health* 18. <https://doi.org/10.3390/ijerph182111291>.
- Nehra, S., Nair, M., Kumar, D., 2019. Hydrothermally shape-controlled synthesis of TiO_2 /graphene for fluoride adsorption studies. *J. Chem. Eng. Data* 64, 5373–5384. <https://doi.org/10.1021/acs.jced.9b00591>.
- Nosaka, Y., Nosaka, A.Y., 2017. Generation and detection of reactive oxygen species in photocatalysis. *Chem. Rev.* 117, 11302 <https://doi.org/10.1021/acs.chemrev.7b00161>.
- Ollis, D.F., 2018. Kinetics of photocatalyzed reactions: five lessons learned. *Front. Chem.* 6, 1–7. <https://doi.org/10.3389/fchem.2018.00378>.
- Orge, C.A., Pereira, M.F.R., Faria, J.L., 2017. Photocatalytic-assisted ozone degradation of metolachlor aqueous solution. *Chem. Eng. J.* 318, 247. <https://doi.org/10.1016/j.cej.2016.06.136>.
- Padmanabhan, N.T., Thomas, N., Louis, J., Mathew, D.T., Ganguly, P., John, H., Pillai, S.C., 2021. Graphene coupled TiO_2 photocatalysts for environmental applications: a review. *Chemosphere* 271, 129506. <https://doi.org/10.1016/j.chemosphere.2020.129506>.
- Pastrana-Martínez, L.M., Morales-Torres, S., Likodimos, V., Figueiredo, J.L., Faria, J.L., Falaras, P., Silva, A.M.T., 2012. Advanced nanostructured photocatalysts based on reduced graphene oxide- TiO_2 composites for degradation of diphenhydramine pharmaceutical and methyl orange dye. *Appl. Catal. B Environ.* 123 (124), 241–256. <https://doi.org/10.1016/j.apcatb.2012.04.045>.
- Pazoki, M., Parsa, M., Farhadpour, R., 2016. Removal of the hormones dexamethasone (DXM) by Ag doped on TiO_2 photocatalysis. *J. Environ. Chem. Eng.* 4, 4426–4434. <https://doi.org/10.1016/j.jece.2016.09.034>.
- Pérez-Molina, Á., Morales-Torres, S., Maldonado-Hódar, F.J., Pastrana-Martínez, L.M., 2020. Functionalized graphene derivatives and TiO_2 for high visible light photodegradation of azo dyes. *Nanomaterials* 10, 1–17. <https://doi.org/10.3390/nano10061106>.
- Pretali, L., Albin, A., Cantalupi, A., Maraschi, F., Nicolis, S., Sturini, M., 2021. TiO_2 -photocatalyzed water depollution, a strong, yet selective depollution method: new evidence from the solar light induced degradation of glucocorticoids in freshwaters. *Appl. Sci.* 11 <https://doi.org/10.3390/app11062486>.
- Qin, Y., Mingce, L., Beihui, T., Baoxue, Z., 2014. RhB adsorption performance of magnetic adsorbent Fe_3O_4 /RGO composite and its regeneration through A fenton-like reaction. *Nano-Micro Lett.* 6, 125. <https://doi.org/10.5101/nml.v6i2.p125-135>.
- Quaresima, A.V., Rubio, K.T.S., Taylor, J.G., Sousa, B.A., Silva, S.Q., Werle, A.A., Afonso, R.J.C.F., 2021. Removal of dexamethasone by oxidative processes: structural characterization of degradation products and estimation of the toxicity. *J. Environ. Chem. Eng.* 9, 106884 <https://doi.org/10.1016/j.jece.2021.106884>.
- Rao, Z., Lu, G., Mahmood, A., Shi, G., Xie, X., Sun, J., 2021. Applied Catalysis B : Environmental Deactivation and Activation Mechanism of TiO_2 and rGO/ Er^{3+} - TiO_2 during Flowing Gaseous VOCs Photodegradation 284, pp. 1–11. <https://doi.org/10.1016/j.apcatb.2020.119813>.
- Rasolevandi, T., Naseri, S., Azarpira, H., Mahvi, A.H., 2019. Photo-degradation of dexamethasone phosphate using UV/Iodine process: kinetics, intermediates, and transformation pathways. *J. Mol. Liq.* 295, 111703 <https://doi.org/10.1016/j.molliq.2019.111703>.
- Rivero, M.J., Ribao, P., Gomez-Ruiz, B., Urriaga, A., Ortiz, I., 2020. Comparative performance of TiO_2 -rGO photocatalyst in the degradation of dichloroacetic and perfluorooctanoic acids. *Sep. Purif. Technol.* 240, 116637 <https://doi.org/10.1016/j.seppur.2020.116637>.
- Rizzo, L., Malato, S., Antakyali, D., Beretsou, V.G., Dolić, M.B., Gernjak, W., Heath, E., Ivancev-Tumbas, I., Karaolia, P., Lado Ribeiro, A.R., Mascolo, G., McArdell, C.S., Schaar, H., Silva, A.M.T., Fatta-Kassinos, D., 2019. Consolidated vs new advanced treatment methods for the removal of contaminants of emerging concern from urban wastewater. *Sci. Total Environ.* 655, 986–1008. <https://doi.org/10.1016/j.scitotenv.2018.11.265>.
- Sabir, R., Waheed, A., Moazzam Ali, M., Mushtaq, U., 2021. Graphene-based photocatalysts for organic pollutant removal from waste-water: recent progress and future challenges. *Environ. Technol. Rev.* 10, 322–340. <https://doi.org/10.1080/21622515.2021.1994658>.
- Saravanan, A., Deivayanai, V.C., Kumar, P.S., Rangasamy, G., Hemavathy, R.V., Harshana, T., Gayathri, N., Alagumalai, K., 2022. A detailed review on advanced oxidation process in treatment of wastewater: mechanism, challenges and future outlook. *Chemosphere* 308, 136524. <https://doi.org/10.1016/j.chemosphere.2022.136524>.
- Serrà, A., Philippe, L., Perreault, F., Garcia-Segura, S., 2021. Photocatalytic treatment of natural waters. Reality or hype? The case of cyanotoxins remediation. *Water Res.* 188 <https://doi.org/10.1016/j.watres.2020.116543>.
- Suriyaraj, S.P., Vijayaraghavan, T., Bijli, P., Selvakumar, R., 2014. Adsorption of fluoride from aqueous solution using different phases of microbially synthesized TiO_2 nanoparticles. *J. Environ. Chem. Eng.* 2, 444–454. <https://doi.org/10.1016/j.jece.2014.01.013>.
- ThermoScientific Knowledge Database. n.d. Titanium [WWW Document]. URL. <https://www.jp.xpsimplified.com/elements/titanium.php>, 2.23.22.
- United States Environmental Protection Agency, 2022. Contaminants of Emerging Concern Including Pharmaceuticals and Personal Care Products [WWW Document]. URL. <https://www.epa.gov/wqc/contaminants-emerging-concern-including-pharmaceuticals-and-personal-care-products>, 12.2.22.
- Vieira Guelfi, D.R., Gozzi, F., Machulek, A., Sirés, I., Brillas, E., de Oliveira, S.C., 2018. Degradation of herbicide S-metolachlor by electrochemical AOPs using a boron-doped diamond anode. *Catal. Today* 313, 182–188. <https://doi.org/10.1016/j.cattod.2017.10.026>.
- Wang, D., Junker, A.L., Sillanpää, M., Jiang, Y., Wei, Z., 2023. Photo-based advanced oxidation processes for zero pollution: where are we now? *Engineering* 23, 19–23. <https://doi.org/10.1016/j.eng.2022.08.005>.
- Wang, F., Zhang, K., 2011. Reduced graphene oxide- TiO_2 nanocomposite with high photocatalytic activity for the degradation of rhodamine B. *J. Mol. Catal. Chem.* 345, 101–107. <https://doi.org/10.1016/j.molcata.2011.05.026>.
- Wang, P., Wang, J., Wang, X., Yu, H., Yu, J., Lei, M., Wang, Y., 2013. One-step synthesis of easy-recycling TiO_2 -rGO nanocomposite photocatalysts with enhanced photocatalytic activity. *Appl. Catal. B Environ.* 132 (133), 452–459. <https://doi.org/10.1016/j.apcatb.2012.12.009>.
- Wang, W., Yu, J., Xiang, Q., Cheng, B., 2012. Enhanced photocatalytic activity of hierarchical macro/mesoporous TiO_2 -graphene composites for photodegradation of acetone in air. *Appl. Catal. B Environ.* 119 (120), 109–116. <https://doi.org/10.1016/j.apcatb.2012.02.035>.
- Xiuling, W., Xiaoxiang, Z., Zhu, Y., 2022. Catalytic degradation of halogenated compounds by synergistic system of metal materials and VB₁₂: a review. *Chem. Ind. Eng. Prog.* 41, 708–720. <https://doi.org/10.16085/j.issn.100-6613.2021-0481>.
- Xu, H.Y., Wu, L.C., Zhao, H., Jin, L.G., Qi, S.Y., 2015. Synergic effect between adsorption and photocatalysis of metal-free g-C₃N₄ derived from different precursors. *PLoS One* 10, 1–20. <https://doi.org/10.1371/journal.pone.0142616>.
- Xu, L., Yang, L., Johansson, E.M.J., Wang, Y., Jin, P., 2018. Photocatalytic activity and mechanism of bisphenol A removal over TiO_2 -x/rGO nanocomposite driven by visible light. *Chem. Eng. J.* 350, 1043–1055. <https://doi.org/10.1016/j.cej.2018.06.046>.
- Yadav, D., Rangabhashiyam, S., Verma, P., Singh, P., Devi, P., Kumar, P., Hussain, C.M., Gaurav, G.K., Kumar, K.S., 2021. Environmental and health impacts of contaminants of emerging concerns: recent treatment challenges and approaches. *Chemosphere* 272, 129492. <https://doi.org/10.1016/j.chemosphere.2020.129492>.
- Yu, H., Xiao, P., Tian, J., Wang, F., Yu, J., 2016. Phenylamine-functionalized rGO/ TiO_2 photocatalysts: spatially separated adsorption sites and tunable photocatalytic selectivity. *ACS Appl. Mater. Interfaces* 8, 29470–29477. <https://doi.org/10.1021/acsami.6b09903>.
- Zazo, J.A., Casas, J.A., Molina, C.B., Quintanilla, A., Rodriguez, J.J., 2007. Evolution of ecotoxicity upon Fenton's oxidation of phenol in water. *Environ. Sci. Technol.* 41, 7164–7170. <https://doi.org/10.1021/es071063l>.
- Zhang, Y., Tang, Z.-R., Fu, X., Xu, Y.-J., 2010. TiO_2 graphene nanocomposites for gas-phase photocatalytic degradation of volatile aromatic pollutant : is TiO_2 -Graphene truly different from other TiO_2 -Carbon composite materials? *ACS Nano* 4, 7303–7314. <https://doi.org/10.1021/nn1024219>.
- Zhao, L., Xu, H., Jiang, B., Huang, Y., 2017. Synergetic photocatalytic nanostructures based on Au/ TiO_2 /reduced graphene oxide for efficient degradation of organic pollutants. *Part. Part. Syst. Charact.* 34 <https://doi.org/10.1002/ppsc.201600323>.